

₁ Study of neutrino-nucleus interaction at around 1 GeV using
₂ a 3D grid-structure neutrino detector, WAGASCI, muon
₃ range detectors and magnetized spectrometer, Baby MIND,
₄ at J-PARC neutrino monitor hall

₅ A. Bonnemaison, R. Cornat, L. Domine, O. Drapier, O. Ferreira, F. Gastaldi,
₆ M. Gonin, J. Imber, M. Licciardi, F. Magniette, T. Mueller, L. Vignoli, and O. Volcy
₇ *Ecole Polytechnique, IN2P3-CNRS, Laboratoire Leprince-Ringuet, Palaiseau,*
₈ *France*

₉ S. Cao and T. Kobayashi

₁₀ *High Energy Accelerator Research Organization (KEK), Tsukuba, Ibaraki, Japan*

₁₁ M. Khabibullin, A. Khotjantsev, A. Kostin, Y. Kudenko, A. Mefodiev, O. Mineev,
₁₂ S. Suvorov, and N. Yershov

₁₃ *Institute for Nuclear Research of the Russian Academy of Sciences, Moscow, Russia*

₁₄ B. Quilain

₁₅ *Kavli Institute for the Physics and Mathematics of the Universe (WPI), The*
₁₆ *University of Tokyo Institutes for Advanced Study, University of Tokyo, Kashiwa,*
₁₇ *Chiba, Japan*

₁₈ T. Hayashino, A. Hiramoto, A.K. Ichikawa, K. Nakamura, T. Nakaya, K Yasutome,
₁₉ and K. Yoshida

₂₀ *Kyoto University, Department of Physics, Kyoto, Japan*

₂₁ Y. Azuma, J. Harada, T. Inoue, K. Kin, N. Kukita, S. Tanaka, Y. Seiya,
₂₂ K. Wakamatsu, and K. Yamamoto

₂₃ *Osaka City University, Department of Physics, Osaka, Japan*

24 A. Blondel, F. Cadoux, Y. Favere, E. Noah, L. Nicola, and S. Parsa

25 *University of Geneva, Section de Physique, DPNC, Geneva, Switzerland*

26 N. Chikuma, F. Hosomi, T. Koga, R. Tamura, and M. Yokoyama

27 *University of Tokyo, Department of Physics, Tokyo, Japan*

28 Y. Hayato

29 *University of Tokyo, Institute for Cosmic Ray Research, Kamioka Observatory,
30 Kamioka, Japan*

31 Y. Asada, K. Matsushita, A. Minamino, K. Okamoto, and D. Yamaguchi

32 *Yokohama National University, Faculty of Engineering, Yokohama, Japan*

33 December 12, 2017

34 **1 Introduction**

35 The understanding of neutrino-nucleus interactions in the 1 GeV energy region is critical
36 for the success of accelerator-based neutrino oscillation experiments such as the T2K exper-
37 iment. Complicated multi-body effects of nuclei render this understanding difficult. The
38 T2K near detectors have been measuring these and significant progress has been achieved.
39 However, the understanding is still limited. One of the big factors preventing from full
40 understanding is the non-monochromatic neutrino beam spectrum. Measurements with
41 different but some overlapping beam spectra would greatly benefit to resolve the contri-
42 bution from different neutrino energies. We, the Wagasci collaboration, proposes to study
43 the neutrino-nucleus interaction at the B2 floor of the neutrino monitor building, where
44 different neutrino spectra can be obtained due to the different off-axis position. Our exper-
45 imental setup contains 3D grid-structure plastic-scintillator detectors filled with water as
46 the neutrino interaction target (Wagasci modules), two side- and one downstream- muon
47 range detectors(MRD's). The 3D grid-structure and side-MRD's allows a measurement of
48 wider-angle scattering than the T2K off-axis near detector (ND280). High water to scintil-
49 lator material ratio enables the measurement of the neutrino interaction on water, which
50 is highly desired for the T2K experiment because it's far detector, Super-Kamiokande,

51 is composed of water. The MRD's consist of plastic scintillators and iron plates. The
52 downstream-MRD, so called the Baby MIND detector, also works as a magnet and pro-
53 vides the charge identification capability as well as magnetic momentum measurement for
54 high energy muons. The charge identification is essentially important to select antineu-
55 trino events in the antineutrino beam because contamination of the neutrino events is as
56 high as 30%. Most of the detectors has been already constructed. The Wagasci modules
57 have been commissioned as the J-PARC T59 experiment and the Baby MIND detector was
58 commissioned at the CERN neutrino platform. Therefore, the collaboration will be ready
59 to proceed to the physics data taking for the T2K beam time in January 2019. We will
60 provide the cross sections of the charged current neutrino and antineutrino interactions on
61 water with slightly higher neutrino energy than T2K ND280 with wide angler acceptance.
62 When combined with ND280 measurements, our measurement would greatly improve the
63 understanding of the neutrino interaction at around 1 GeV and contribute to reduce one
64 of the most significant uncertainty of the T2K experiment.

65 **2 Experimental Setup**

66 Figure. 1 shows a schematic view of the entire set of detectors. A central detector, Wagasci
67 modules, consists of 3D grid-structure plastic-scintillator detectors filled with water as the
68 neutrino interaction target. They are surrounded by two side- and one downstream- muon
69 range detectors(MRD's) The MRD's are used to select muon tracks from the charged-
70 current (CC) interactions and to reject short tracks caused by neutral particles that orig-
71 inate mainly from neutrino interactions in material surrounding the central detector, like
72 the walls of the detector hall, neutrons and gammas, or neutral-current (NC) interactions.
73 The muon momentum can be reconstructed from its range inside the detector. The MRD's
74 consist of plastic scintillators and iron plates. In addition, each of the iron plates of the
75 downstream-MRD, so called the Baby MIND detector, is wound by a coil and can be
76 magnetized. It provide the charge selection capability.

77 For all detectors, scintillation light in the scintillator bar is collected and transported
78 to a photodetector with a wavelength shifting fiber (WLS fiber). The light is read out by
79 a photodetector, Multi-Pixel Photon Counter (MPPC), attached to one end of the WLS
80 fiber. The signal from the MPPC is read out by the dedicated electronics developed for the
81 test experiment to enable bunch separation in the beam spill. The readout electronics is
82 triggered using the beam-timing signal from MR to synchronize to the beam. The beam-
83 timing signal is branched from those for T2K, and will not cause any effect on the T2K
84 data taking.

85 T2K adopted the off-axis beam method, in which the neutrino beam is intentionally
86 directed 2.5 degrees away from SK producing a narrow band ν_μ beam. The off-axis near
87 detector, ND280, is installed towards the SK direction in the B1 floor of the near detector
88 hall of the J-PARC neutrino beam-line. We propose to install our detector in the B2 floor

tmp.pdf

Figure 1: Schematic view of entire sets of detectors.

89 of the near detector hall, where the off-axis angle is similar but slightly different: 1.5 degree.
90 The candidate detector position in the B2 floor is shown in Fig. 2. The expected neutrino
91 energy spectrum at the candidate position is shown in Fig. 3.

92 **2.1 Wagasci module**

93 The dimension of the each Wagasci module is 100cm \times 100cm in the x and y directions
94 and 50cm along the beam direction. Inside the Wagasci module, plastic scintillator bars
95 are aligned as a 3D grid-like structure, shown in Fig. 5, and spaces in the structure are
96 filled with water for the water-in Wagasci module.

97 The total water mass serving as neutrino targets are \sim 0.5 ton. When neutrinos interact
98 with hydrogen, oxygen or carbon, in water and scintillators, charged particles are generated.
99 Neutrino interactions are identified by detecting tracks of charged particles through plastic
100 scintillation bars. Thanks to the 3 D grid-like structure of the scintillator bars, the Wagasci
101 module has 4π angular acceptance for charged particles. Furthermore, adopting a 5cm grid
102 spacing, short tracks originated from protons and charged pions can be reconstructed with
103 high efficiency. Thin plastic scintillator bars (thickness \sim 0.3cm) are used for the Wagasci
104 module to reduce the mass ratio of scintillator bars to water, because neutrino interactions
105 in the scintillator bars are a background for the cross section measurements. Scintillator
106 bars whose dimensions are 2.5cm \times 0.3cm \times 100cm are used for the Wagasci module. The
107 total number of channels in one Wagasci module is 1280.

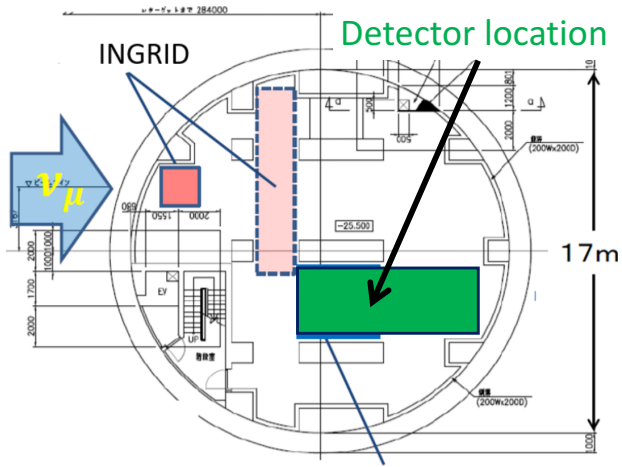


Figure 2: Candidate detector position in the B2 floor of the near detector hall.

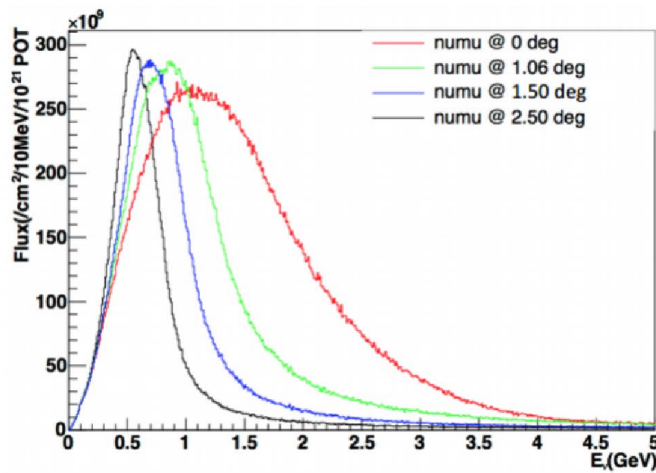


Figure 3: Neutrino energy spectrum at the candidate detector position(red, off-axis 1.5 degree). The spectrum at the ND280 site (black, off-axis 2.5 degree) is also shown.

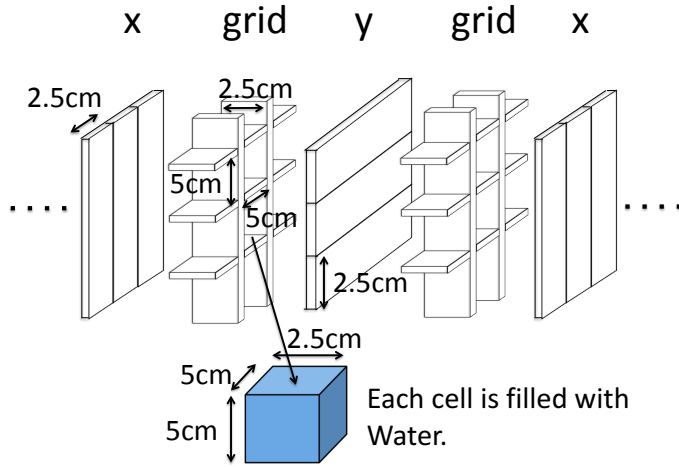


Figure 4: Schematic view of 3D grid-like structure of plastic scintillator bars inside the central detector.

108 2.2 INGRID Proton module

109 INGRID Proton module is a neutrino detectors of the T2K experiment. It is composed only
110 with scintillator bars in its tracking region. (Add more explanation here.) It was installed
111 at the neutrino beam axis on the SS floor of the T2K near detector hall in 2010, and had
112 been used for neutrino cross section measurements. In August 2017, it was moved to the
113 B2 floor of the same detector hall by J-PARC T59 after getting the approval from T2K
114 to use them. J-PARC T59 is performing neutrino beam measurement using the detector
115 from October 2017, and the measurement will continue until May 2018.

116 2.3 Baby MIND

117 The Baby MIND is the downstream Muon Range Detector. It also works as a magnet and
118 provides the charge identification capability as well as magnetic momentum measurement
119 for high energy muons.

120 The Baby MIND collaboration ¹ submitted a proposal to the SPSC at CERN, SPSC-P-
121 353. The project was approved by the CERN research board as Neutrino Platform project
122 NP05 and constructed. The detector consists of 33 magnet modules, each 3500 mm ×
123 2000 mm × 50 mm (30 mm steel) with a mass of approximately 2 tonnes. Of these magnet
124 modules, 18 are instrumented with plastic scintillator modules.

¹Contact person: E. Noah, Spokesperson: A. Blondel, Deputy spokesperson: Y. Kudenko

tmp.pdf

Figure 5: tmp.

125 **2.3.1 Magnet modules**

126 The Baby MIND is built from sheets of iron interleaved with scintillator detector modules
127 but unlike traditional layouts for magnetized iron neutrino detectors (e.g. MINOS) which
128 tend to be monolithic blocks with a unique pitch between consecutive steel segments and
129 large conductor coils threaded around the whole magnet volume, the Baby MIND iron seg-
130 ments are all individually magnetized as shown in Fig. 6, allowing for far greater flexibility
131 in the setting of the pitch between segments, and in the allowable geometries that these
132 detectors can take.

133 The key design outcome is a highly optimized magnetic field map. A double-slit con-
134 figuration for coil winding was adopted to increase the area over which the magnetic flux
135 lines are homogeneous in B_x across the central tracking region. Simulations show the
136 magnet field map to be very uniform over this central tracking region covering an area of
137 $2800 \times 2000 \text{ mm}^2$, Fig. 7. The B_x component dominates in this region, with negligible B_y
138 and B_z . This was confirmed by measuring the field with 9 pick-up coils wound around
139 the first module. Subsequent modules were equipped with one pick-up coil. Test results
140 on the 33 modules show all to achieve the required field of 1.5 T for a current of 140 A,
141 with a total power consumption of 11.5 kW. The polarity of the field map shown in Fig. 7
142 (middle) can be reversed by changing the power supply configuration.

143 **2.3.2 Scintillator modules**

144 Each of the 18 scintillator modules is constructed from 2 planes of horizontal counters (95
145 counters in total) and 2 planes of vertical counters (16 counters in total) [2], arranged
146 with an overlap between planes to achieve close to 100% hit efficiency for minimum ioniz-
147 ing muons. The arrangement of planes within a module is vertical-horizontal-horizontal-
148 vertical. This arrangement was the result of an assembly approach whereby each plane

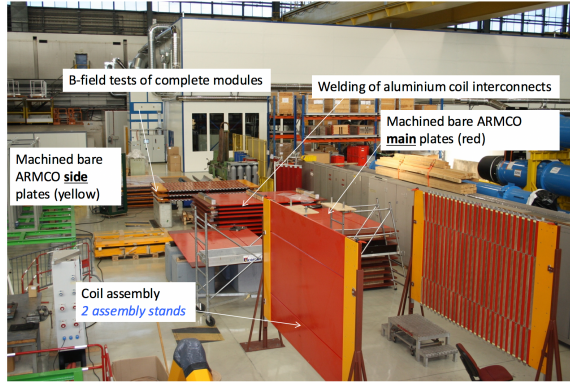


Figure 6: Magnet assembly zone at CERN.

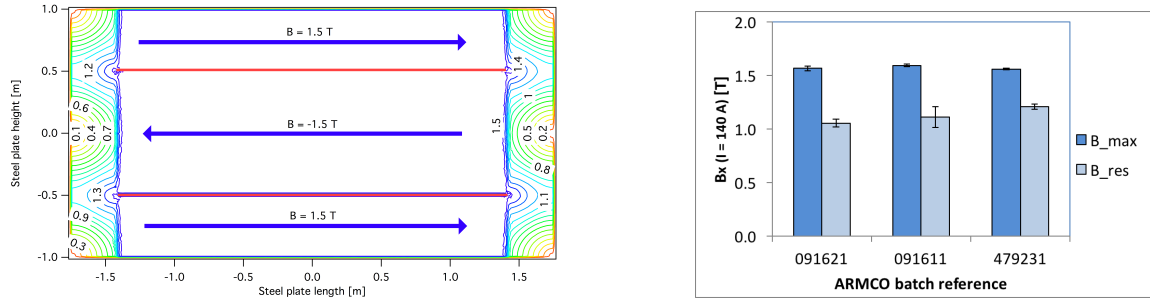


Figure 7: Left) Magnetic field map with a coil along 280 cm of the length of the plate. Right) Measured B field for 33 modules.

149 was built from 2 half-planes, with each half plane consisting of a horizontal plane and a
 150 vertical plane. The scintillator bars are held in place using structural ladders that align and
 151 maintain the counters, Fig. 8. No glue is used in the process, so counters can be replaced.
 152 Aluminum sheets front and back provide light tightness.

153 The plastic scintillator counters were made from 220 mm-wide slabs, consisting of
 154 extruded polystyrene doped with 1.5% paraterphenyl (PTP) and 0.01% POPOP. They were
 155 cut to size then covered with a 30-100 μm thick diffuse reflector resulting from etching of
 156 the surface with a chemical agent [4, 5]. The horizontal counter size is $2880 \times 31 \times 7.5 \text{ mm}^3$,
 157 with one groove along the length of the bar in which sits a wavelength shifting fiber from
 158 Kuraray. The vertical counter size is $1950 \times 210 \times 7.5 \text{ mm}^3$, with one U-shaped groove
 159 along the bar. On each counter, two custom connectors house silicon photomultipliers,
 160 MPPC type S12571-025C from Hamamatsu, either side of the horizontal counter, and
 161 both connectors at the top for the vertical counter. This geometrical configuration for
 162 vertical counters was chosen for ease of connectivity to the electronics, and maintenance
 163 operations.



Figure 8: Scintillator modules assembly. Left) top of front half-module showing vertical counters, and the spacers-ladders that set the pitch between horizontal counters and hold them in place. Middle) rear half-module showing horizontal counters on their ladders. Right) Assembled rear half-module, the front half-module can be seen in the background.

164 A total of 1744 horizontal counters and 315 vertical counters (including spares) were
 165 produced at the Uniplast company (Vladimir, Russia).

166 2.3.3 Electronics

167 The Baby MIND electronic readout scheme includes several custom-designed boards [6].
 168 The revised version is shown in Fig. 9. At the heart of the system is the electronics
 169 Front End Board (FEB), developed by the University of Geneva. The readout system
 170 includes two ancillary boards, the Backplane, and the Master Clock Board (MCB) whose
 171 development has been managed by INRNE (Bulgarian Academy of Sciences) collaborators.

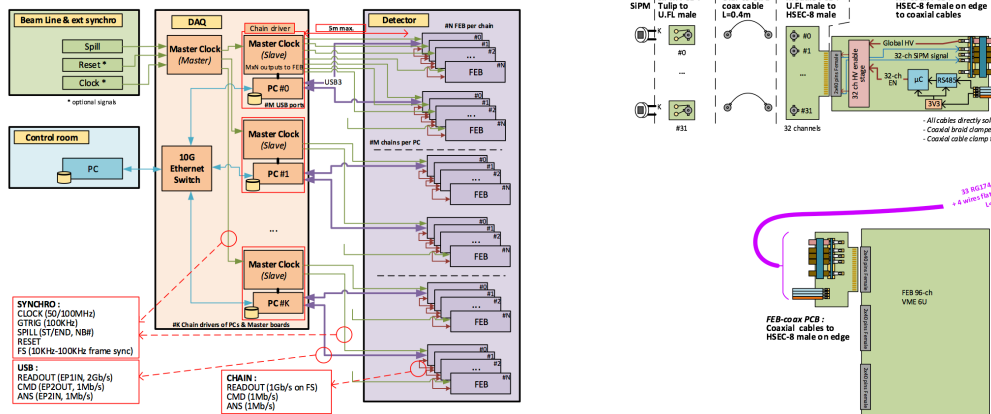


Figure 9: Left) Baby MIND electronics readout scheme. Right) SiPM-to-FEB connectivity.

172 The FEBv2 hosts 3 CITIROC chips that can each read in signals from 32 SiPMs [3].
 173 Each signal input is processed by a high gain, and a separate low gain, signal path. The
 174 outputs from the slow shapers can be sampled using one of two modes: a mode with an

externally applied delay, and a peak detector mode. A faster shaper can be switched to either HG or LG paths, followed by discriminators with adjustable thresholds providing 32 individual trigger outputs and one OR32 trigger output. An Altera ARIA5 FPGA on the FEBv2 samples these trigger outputs at 400 MHz, recording rising and falling times for the individual triggers and assigning time stamps to these. Time-over-threshold from the difference between falling and rising times gives some measure of signal amplitude, used in addition to charge information and useful if there is more than one hit per bar within the deadtime due to the readout of the multiplexed charge output of $\sim 9 \mu\text{s}$. The ARIA5 also manages the digitization of the sampled CITIROC multiplexed HG and LG outputs via a 12-bit 8-ch ADC.

The internal 400 MHz clock on the FEBv2 can be synchronized to a common 100 MHz clock. The synchronization subsystem combines input signals from the beam line into a digital synchronization signal (SYNC) and produces a common detector clock (CLK) which can eventually be synchronised to an external experiment clock. Both SYNC and CLK signals are distributed to the FEBs. Tests show the FEB-to-FEB CLK(SYNC) delay difference to be 50 ps (70 ps). Signals from the beam line at WAGASCI include two separate timing signals, arriving 100 ms and $30 \mu\text{s}$ before the neutrino beam at the near detectors. The spill number is available as a 16-bit signal.

The Baby MIND construction was completed in June 2017, and it was then tested in June and July 2017 at the Proton Synchrotron experimental hall at CERN with a mixed particle beam comprising mostly muons whose momenta could be selected between 0.5 and 5 GeV/c. An event display from the summer 2017 tests is shown in Fig. 10. All counters were measured at INR Moscow with a cosmic ray setup using the same type S12571-025C MPPCs and CAEN DT5742 digitizer [?]. The average light yield (sum from both ends) was measured to be 37.5 photo-electrons (p.e.) per minimum ionizing particle (MIP) and 65 p.e./MIP for vertical and horizontal counters, respectively. After shipment to CERN, all counters were tested once more individually with an LED test setup [?]. 0.1% of counters failed the LED tests and were therefore not used during the assembly of modules.

2.4 Side muon range detector

Four Side-MRD modules for tracking secondary particles from neutrino interactions will be constructed by the end of January 2018. Each Side-MRD module is composed of 11 steel plates and 10 layers of total 80 scintillator slabs installed in 13 mm gaps between the 30 mm thick plates. Each steel plate size is $30 \times 1610 \times 1800 \text{ mm}^3$. Total module size is $2236 \times 1630 \times 975 \text{ mm}^3$ as shown in Fig. 11, weight is ~ 8.5 ton.

Scintillator bars were manufactured by Uniplast company in Vladimir, Russia. Polystyrene based scintillators were extruded with thickness of 7 mm, then cut to the size of $7 \times 200 \times 1800 \text{ mm}^3$. Dopant composition is 1.5% PTP and 0.01% POPOP. Scintillator surface was etched by a chemical agent to form a white diffuse layer with excellent reflective performance. Ideal contact between the scintillator and the reflector raises the light yield up to

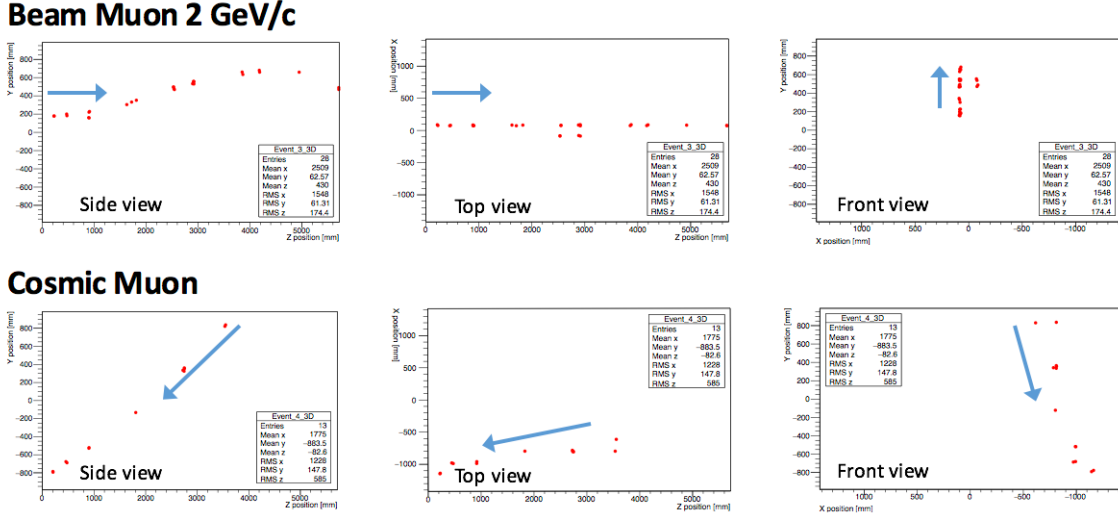


Figure 10: Comparison of a beam muon and cosmic muon in the three different geometrical projections of the detector. The beam impinges on the detector from the left. The arrows indicate the direction of travel of these muons. The direction of the cosmic muon is inferred from timing information.

214 50% comparing to an uncovered scintillator. Sine like groove was milled along the scin-
 215 tillator to provide uniform light collection over the whole scintillator surface. WLS Y11
 216 Kuraray fiber of 1 mm diameter is glued with an optical cement EJ-500 in the S-shape
 217 groove as shown in Fig. 12. Bending radius is fixed to 30 mm that was specified to be safe
 218 for Kuraray S-type fibers. Both ends of the fiber are glued into optical connectors (Fig.
 219 13) which mounted within a scintillator body.

220 The plastic molded connectors provide an interface to SiPMs, Hamamatsu MPPC
 221 S13081-050CS(X1) used for the WAGASCI detector. Optical coupler of this type (so-called
 222 Baby-mind type of optical connector) consists of two parts (see Fig. 13): an container for
 223 the MPPC and a ferrule with the fiber. The ferrule is glued in the scintillator, and its end
 224 with glued in WLS fiber was polished. Both parts of the optical coupler are latched by a
 225 snap-like mechanism: a locking groove inside the container and matching ring protuber-
 226 ance on the ferrule. To ensure the optical contact a foam spring made of sponge rubber
 227 presses the MPPC to the fiber end (Fig. 14).

228 Scintillators for the Side-MRD modules had been assembled at INR in Russia, and
 229 shipped to Japan in July 2017. The light yield for each scintillator was measured with
 230 cosmic rays at INR and at YNU in Japan after delivery. Parameters measured at the
 231 center of the counter were : the light yields LY_1 and LY_2 at both ends, the light yield
 232 asymmetry between the ends calculated as $100\% \times \frac{LY_1 - LY_2}{LY_1 + LY_2}$. After tests at INR we selected
 233 324 counters from measured 332 ones with the mean light yield of 45 p.e./MIP ($LY_1 + LY_2$

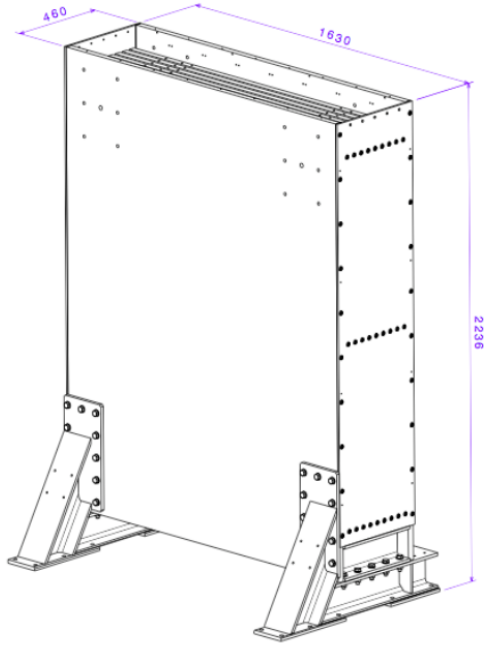


Figure 11: Support structure of the Side-MRD module.

) and the asymmetry value less than 10 %. The measuremens at YNU yielded the average total light yield of about 40 p.e./MIP which varies in range from 32 to 50 p.e/MIP (Fig. 15 (left)). Only two counters showed relatively high asymmetry close to 25 % as shown in Fig. 15 (right). Using the results of the quality assurance test we selected 320 scintillator counters for the Side-MRD modules.

We also measured the time resolution for a combination of four counters piled each on another one. Time resolution for a single counter is determined as rms of $(T_{left} - T_{right})/2$ distribution. The difference of times was chosen to remove the correlated time fluctuation caused by a start trigger signal. The average result for four counters is $\sigma_T = 1.04$ ns (Upper left plot in Fig. 16). For a set of n counters the time resolution is calculated as $\frac{(T_L - T_R)_1 + (T_L - T_R)_2 + \dots + (T_L - T_R)_n}{2 \times n}$. The result of combination of 2, 3, 4 counters is 0.79 ns, 0.66 ns and 0.58 ns, correspondently (Fig. 16).

Construction of Side-MRD modules will be done from November 2017 to January 2018 at Yokohama National University, then they will be transported to J-PARC and will be installed at B2 floor of the T2K near detector hall before T2K beam in March 2018.

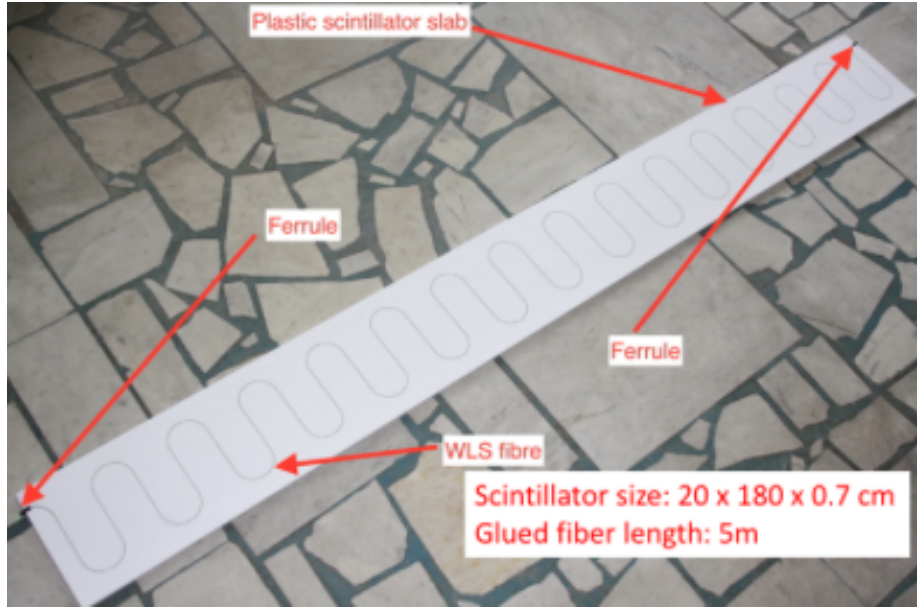


Figure 12: Scintillator bar of the Side-MRD modules.

²⁴⁹ 3 Physics goals

²⁵⁰ We will measure the differential cross section for the charged current interaction on H₂O
²⁵¹ and Hydrocarbon(CH)). The water-scintillator mass ratio of the Wagasci module is as
²⁵² high as 5:1 and the high purity measurement of the cross section on H₂O is possible. One
²⁵³ experimental option is to remove water from one of the two Wagasci modules. The water-
²⁵⁴ out WAGASCI module will allow to measure pure-CH target interactions with very low
²⁵⁵ momentum-threshold for protons. It will also benefit to subtract the background from
²⁵⁶ interaction with scintillator in the water target measurement. Another option is to add
²⁵⁷ the T2K proton module which is fully made of plastic scintillators. It will allow the high
²⁵⁸ statistics comparison of cross section between H₂O and CH and also comparison with
²⁵⁹ the ND280 measurement. The actual configuration will be optimized with detailed MC
²⁶⁰ simulation by 2018 Summer.

²⁶¹ Our setup allows the measurements of inclusive and also exclusive channels such as 1- μ ,
²⁶² 1- $\mu 1p$, 1- $\mu 1\pi \pm np$ samples, former two of which are mainly caused by the quasi-elastic and
²⁶³ 2p2h interaction and the latter is mainly caused by resonant or coherent pion production
²⁶⁴ and deep elastic scattering. In general, an accelerator produced neutrino beam spectrum
²⁶⁵ is wide and the energy reconstruction somehow rely on the neutrino interaction model.

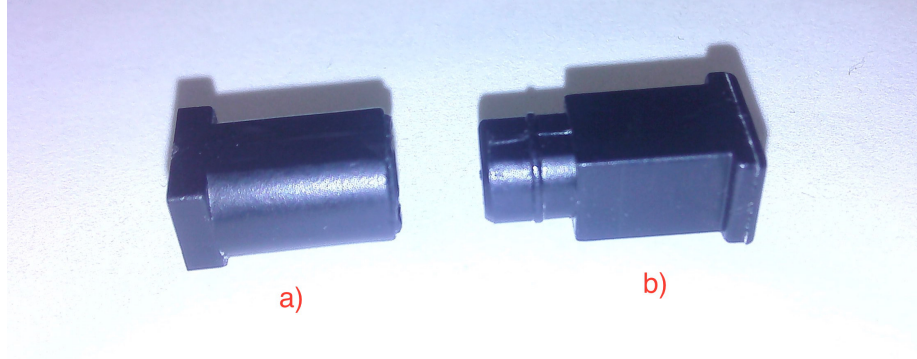


Figure 13: Optical connector for the Side-MRD scintillator. a) MPPC cover. b) Ferrule.

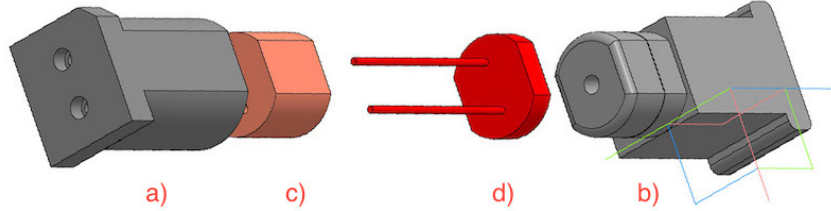


Figure 14: Scheme of the MPPC placement in optical connector. a) MPPC cover. b) Ferrule. c) Spring (sponge rubber). d) MPPC.

266 Therefore, recent neutrino cross section measurement results including those from T2K
 267 are given as a flux-integrated cross section rather than cross sections as a function of
 268 the neutrino energy to avoid the model dependency. We can provide the flux-averaged
 269 cross section. In addition, by combining our measurements with those at ND280, model-
 270 independent extraction of the cross section for narrow energy region becomes possible.
 271 This method was demonstrated in [1] and also proposed by P** (NUPRISM).

272 3.1 Expected number of events

273 Expected number of neutrino events after the event selections is evaluated with Monte
 274 Carlo simulations as we will discuss in Section 5. 2.41×10^4 CC events are expected in
 275 two WAGASCI modules after the selection with 1×10^{20} POT in neutrino-mode, and its
 276 purity is 75.5 %. In case we choose the option with one WAGASCI module and the T2K
 277 proton module, 1.2×10^4 CC events are expected in the WAGASCI module and $\sim 1 \times 10^4$
 278 CC events are expected in the T2K proton module. In case we choose the option with one

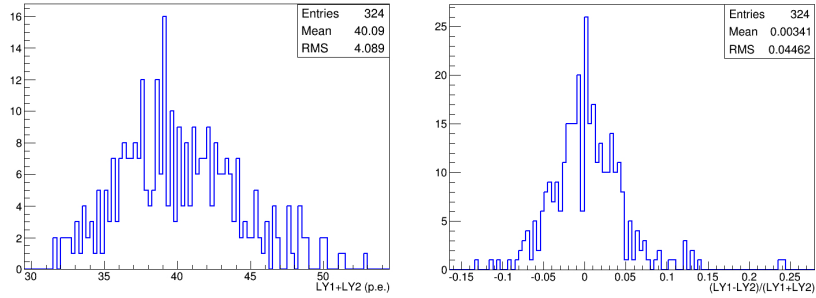


Figure 15: Total light yield distribution (left) and light yield assymetry (right) measured at YNU.

water-in WAGASCI module and one water-out WAGASCI module, 1.2×10^4 CC events are expected in the water-in module and 0.24×10^4 CC events are expected in the water-out module.

3.2 Pseudo-monochromatic beam by using different off-axis fluxes

The off-axis method gives narrower neutrino spectrum, and the peak energy is lower for larger off-axis angle. There still remains high energy tail mainly due to neutrinos from Kaon decay. The off-axis angle of the Wagasci location is 1.5 degree and different from the ND280 2.5 degree. Top two plots of Fig. 17 show the energy spectra of fluxes and neutrino interaction events at these two different location. The high energy tail of ND280 flux can be somehow subtraction by using the Wagasci measurement. The low energy part of the Wagasci flux can be also subtracted by using the ND280 measurement. Bottom two plots of Fig. 17 demonstrate this method. We can effectively get two fluxes, from 0.2 GeV to 0.9 GeV and 0.6 GeV and 2 GeV and measure flux-integrated cross section for these two fluxes.

3.3 Subjects Wagasci can contribute

In T2K experiment, neutrinos interact with bound nucleons in relatively heavy nuclei (Carbon and Oxygen), so the cross-section is largely affected by nuclear effects. The nuclear effects are categorized as nucleons' momentum distribution in nucleus, interactions with correlated pairs of nucleons in nucleus (two particles-two holes, 2p2h), collective nuclear effects calculated with Random Phase Approximation (RPA) and final state interactions (FSI) of secondary particles in the nuclei after the initial neutrino interactions.

The 2p2h interactions mainly happen through Δ resonance interactions following a pion-less decay and interactions with a correlated nucleon pair. The 2p2h interactions are



fig/side_mrd_combi_time.pdf

Figure 16: Time resolution for one (upper left) and a set of 2,3,4 Side-MRD counters.

302 observed in electron scattering experiments (add ref. here) where the 2p2h events observed
303 in the gap between Quasi-Elastic region and Pion-production region as shown in Fig. ??.
304 Neutrino experiments also attempt to measure the 2p2h interactions, but separation of the
305 QE peak and the 2p2h peak is more difficult because transferred momentum (p) and energy
306 (w) are largely affected by neutrino energies which cannot be determined event-by-event in
307 the wide energy spectrum of the accelerator neutrino beam. Our model-independent narrow
308 neutrino spectra extracted from combined analyses of our data and ND280 data are ideal
309 for searching the 2p2h interaction because clearer separation of the QE peak and the 2p2h
310 peak is expected. Another way to observe the 2p2h interaction is direct measurement of
311 proton tracks in CC 0π sample with low detection threshold and full acceptance. Fig. ??
312 shows proton multiplicities in CCQE events and 2p2h events, and Fig. ?? shows opening

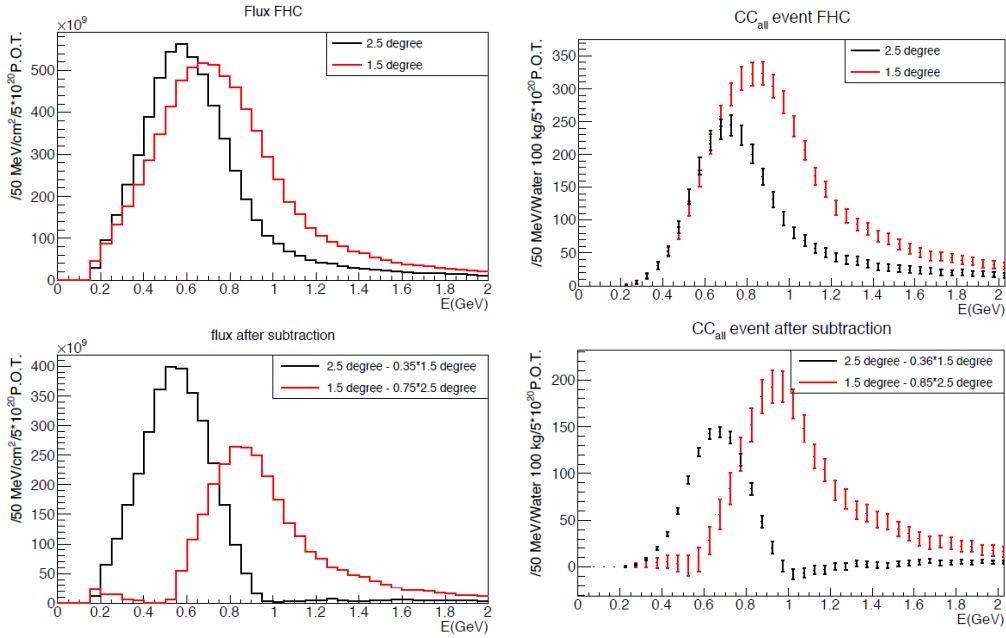


Figure 17: Energy spectra obtained by using different off-axis angle fluxes. Top two plots show the fluxes(left) and spectra of interaction events (right) for ND280 (off-axis 2.5 degree) and Wagasci (off-axis 1.5 degree). Bottom two plots show the fluxes (left) and spectra of interaction events (right) obtained by subtraction of fluxes at ND280 and Wagasci. The error bar is for the statistical error and those in the bottom right plot is obtained assuming the statistical error for ND280 measurement is much smaller than that of Wagasci experiment.

angles among two proton tracks in the same samples. The water-out WAGASCI can provide good sample for the 2p2h interaction search because its low density medium enables the detection of low momentum protons in addition to the full acceptance.

The corrections from collective nuclear effects calculated by RPA as a function of Q^2 are shown in Fig. ???. The Q^2 dependence of the correction can be tested by measuring angular distribution of muons in CC1- μ and CC1- $\mu 1p$ events. The uncertainties of the corrections in low (high) Q^2 regions can be constrained by observing the events with a forward-going (high-angle) muon, so it is essential to measure muon tracks with full acceptance.

T2K experiment is starting to use ν_e CC1 π events for its CP violation search to increase the statistics. One of the biggest uncertainty of the CC1 π sample comes from the final state interactions of pions in the nuclei after the initial neutrino interactions because they change the multiplicity, charge and kinematics of the pions. The multi-pion production events can be migrated into the CC1 π sample due to the FSIs, and they become important

326 backgrounds. We can constrain the uncertainties from the pion FSIs by measuring pion
 327 rescattering in the detector and pion multiplicity in ν_μ CCn π sample with low detection
 328 threshold and full acceptance for pion tracks. The water-out WAGASCI can provide good
 329 sample for the pion FSI studies because its low density medium enables the detection of
 330 low momentum pions in addition to the full acceptance.

331 4 Status of J-PARC T59 experiment

332 We had submitted a proposal of a test experiment to J-PARC in April 2014 to test a new
 333 detector with a water target, WAGASCI, at the neutrino monitor hall, and the proposal
 334 was approved as J-PARC T59. The project contains the side and downstream muon range
 335 detectors as well.

336 The first WAGASCI module has been constructed in 2016 and installed at the on-
 337 axis position in front of the T2K INGRID detector for the commissioning and the first
 338 cross section measurement as a part of the T2K experiment. The INGRID electronics
 339 boards are used to read the signal. The light yield measured with muons produced by
 340 the interaction of neutrinos in the hall wall, shown in Fig. 18, is sufficiently high to get
 good hit efficiency. A track search algorithm based on the cellular automaton has been

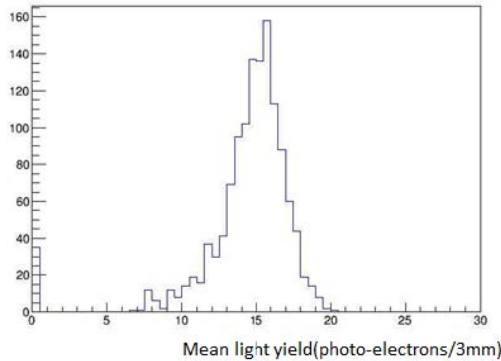


Figure 18: Light yield for muons produced by the interaction of neutrinos in the hall wall. Average light yields for each channel are plotted.

341
 342 developed using the software tools by the T2K INGRID. Examples of observed events are
 343 shown in Fig. 19 The tracking efficiency in 2-dimensional projected plane was evaluated
 344 by comparing the reconstructed track in the WAGASCI module and the INGRID module
 345 and shown in Fig.20. Note that that the tracking efficiency for high angle (> 70 deg) is not
 346 evaluated because of the acceptance of the INGRID module, not because of the limitation
 347 of the WAGASCI module.

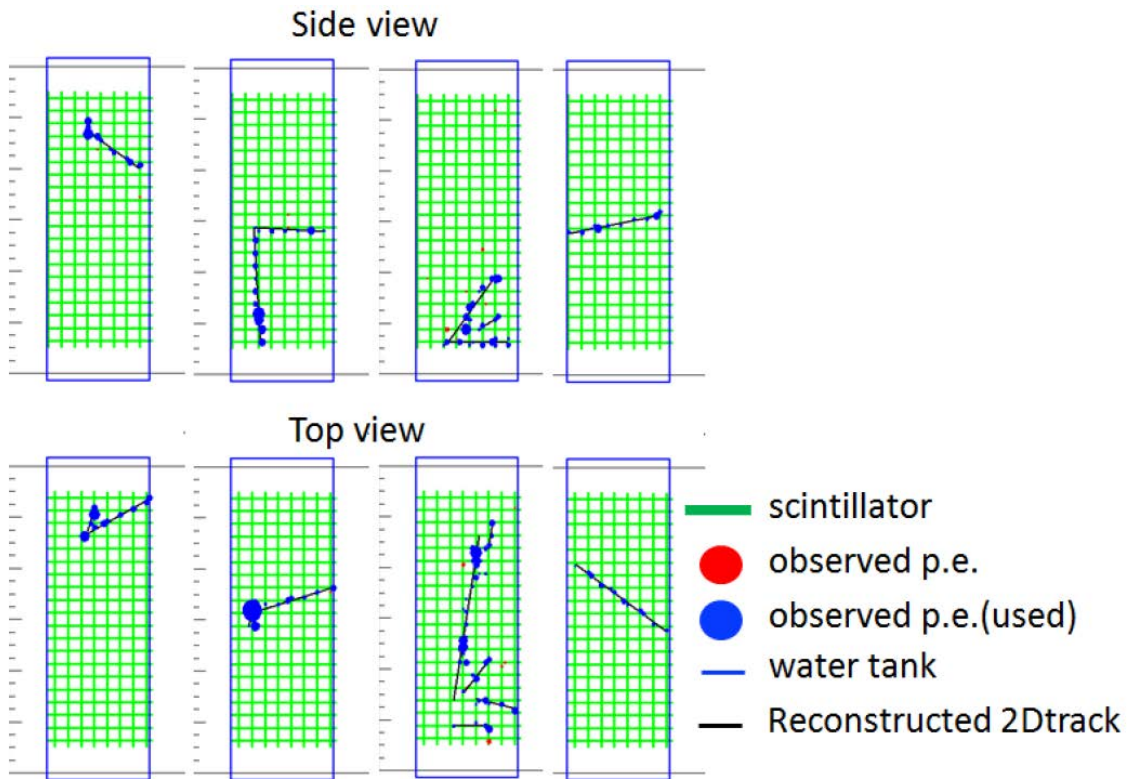


Figure 19: Example event displays of the WAGASCI module at on-axis. The reconstructed tracks are overlaid.

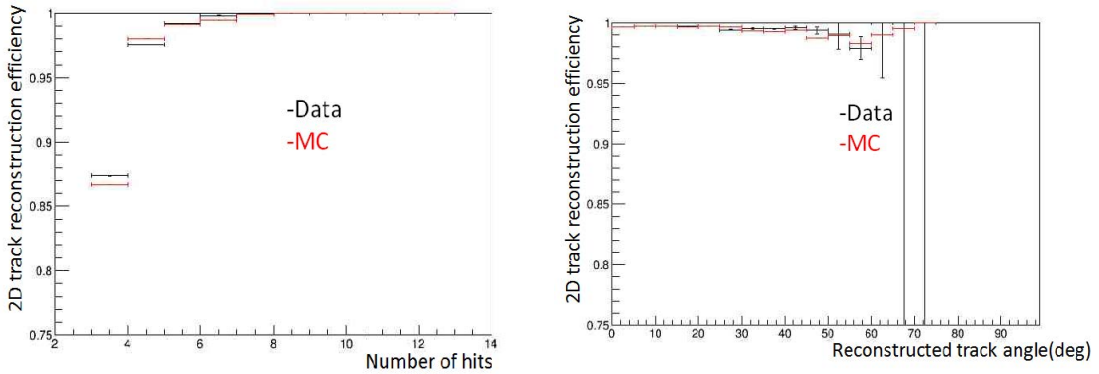


Figure 20: 2D track reconstruction efficiency as a function of number of hits (left) and track angle (right). Here the track angle is the one reconstructed by the INGRID module.

348 In 2017 Autumn, the construction of the second WAGASCI module and the dedicated
 349 electronics board were completed. The module and the electronics were install to the B2
 350 floor together with the T2K proton module and the INGRID module as shown in Fig. 21.
 351 The proton module is to be used as the entering muon veto and also for the comparison
 352 of interaction between CH and Water. The INGRID module is for the temporary muon
 353 detector with limited acceptance for this period. The detector was commissioned and is
 354 in operation to take data with the antineutrino beam during the T2K beam time from
 355 October.

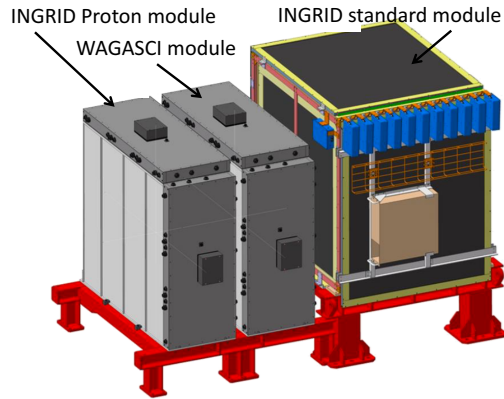


Figure 21: J-PARC T59 detector configuration in October 2017.

356 The production of the components of the side muon range detectors has been completed
357 and now the detectors are being assembled at the Yokohama National University. These
358 detectors will be installed sometime from January to June, 2018 when T2K is not running.

359 The Baby MIND detector was transported from CERN to Japan in December, 2017.
360 It will be installed and commissioned in Jan.-Feb. 2018 and T59 will take the neutrino-
361 induced muon data in April and May.

362 5 MC studies

363 5.1 Detector simulation

364 Expected number of neutrino events in the WAGASCI detector is evaluated with Monte
365 Carlo simulations. Neutrino beam flux at the detector location is simulated by T2K neutrino
366 flux generator, JNUBEAM, neutrino interactions with target materials are simulated
367 by a neutrino interaction simulator, NEUT, detector responses are simulated using
368 GEANT4-based simulation. The neutrino flux at the detector location, 1.5 degrees away
369 from the J-PARC neutrino beam axis, is shown in Figure 3, and its mean neutrino energy
370 is around 0.68 GeV.

371 5.1.1 Detector geometry

372 The detector geometry in the GEANT4-based simulation is slightly different from the
373 actual detector as shown in Fig. 23. The active neutrino target region consists of four
374 WAGASCI modules, and each WAGASCI detector has the dimension with 100 cm × 100
375 cm in the x and y directions and 50 cm along the beam direction. An event display of a
376 MC event in the WAGASCI detectors is shown in Figure ???. Two Side-MRD modules is
377 installed at both sides of the WAGASCI modules, and each Side-MRD module consists of
378 ten iron plates whose dimension is 3 cm (thickness) × 180 cm (height) × 320 cm (width).
379 The distance between the Side-MRD modules and WAGASCI modules is 60 cm. The
380 downstream-MRD equivalent to the Baby-MIND is installed at the downstream of the
381 WAGASCI modules. The downstream-MRD consists of ten iron plates whose dimension is
382 3 cm (thickness) × 180 cm (height) × 320 cm (width) and another ten iron plates whose
383 dimension is 6 cm (thickness) × 180 cm (height) × 320 cm (width). The distance between
384 the downstream-MRD modules and WAGASCI modules is 60 cm.

385 In order to estimate backgrounds from neutrino interactions in the wall and floor of the
386 experimental hall, the geometry of the experimental hall is implemented in the GEANT4-
387 based detector simulation.

388 5.1.2 Response of detector components

389 The energy deposit inside the scintillator is converted into the number of photons. The
390 effects of collection and attenuation of the light in the scintillator and the WLS fiber are

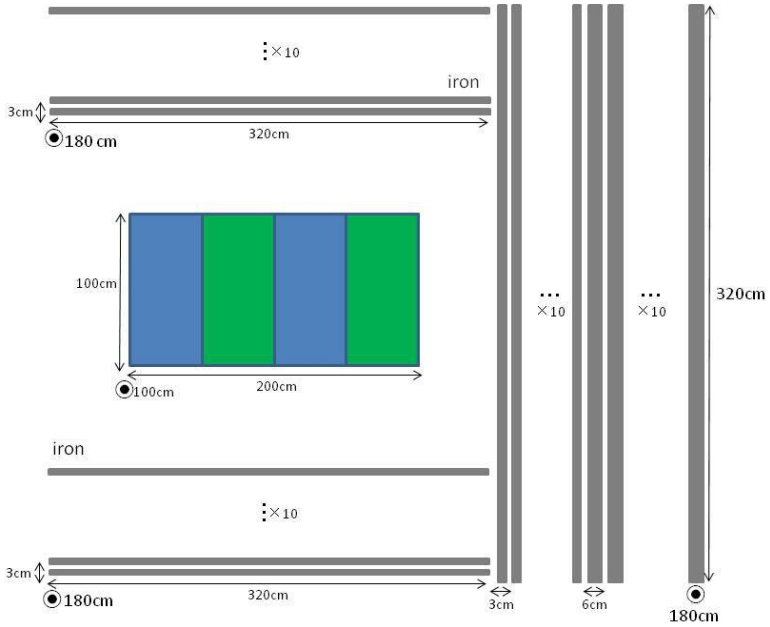


Figure 22: Geometry of the detectors in the Monte Carlo simulation.

391 simulated, and the MPPC response is also taken into account. The light yield is smeared
 392 according to statistical fluctuations and electrical noise.

393 5.2 Track reconstruction

394 To select neutrino interaction from the hit patterns, a track reconstruction algorithm is
 395 developed. The flow of the track reconstruction is as follows.

396 1. Two-dimensional track reconstruction in each sub-detectors

397 2. Track matching among the sub-detectors

398 3. Three -dimensional track reconstruction

399 Add explanation about two-dim reco, track matching and three-dim reco here.

400 5.3 Event selection

401 First, the events with the track which starts in 5 cm from the wall of the WAGASCI module
 402 are rejected to remove the background from the outside.

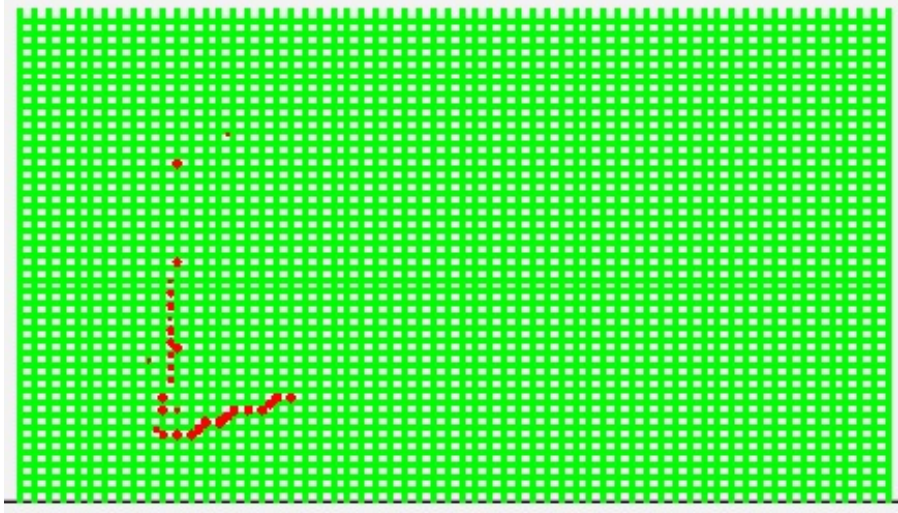


Figure 23: An event display of MC event in WAGASCI detectors. Green lines are scintillators and red circles are the hit channels.

403 Second, to reject backgrounds from NC and neutral particles, the longest tracks are
 404 required to penetrate more than one (five) iron plates in Side-MRD modules (Baby-MIND).
 405 Then, in order to measure muon momentum, the longest tracks are required to stop in
 406 MRDs (Side-MRD modules and Baby-MIND) or penetrate all iron plates.

407 Table 1 and 2 show numbers of the selected events after each event election in neutrino-
 408 mode and antineutrino-mode respectively. As for the neutrino-mode, 2.12×10^4 CC events
 409 are expected with 1×10^{21} POT, and the purity is 81.3 %. The main background for
 410 the neutrino-mode is the neutrino interactions in the scintillators inside the WAGASCI
 411 detector. As for the antineutrino-mode, 0.83×10^4 CC events are expected with $1 \times$
 412 10^{21} POT, and the purity is 62.0 %. The main background for the antineutrino-mode
 413 is the wrong sign contamination from ν_μ events and the antineutrino interactions in the
 414 scintillators inside the WAGASCI detector.

415 Figure 24 and 25 show the reconstructed angles of the longest tracks in the selected
 416 events in the neutrino-mode and the anti-neutrino mode respectively.

417 Figure 26 and 27 show the iron plane numbers corresponding to the end points of the
 418 longest tracks in the selected events.

419 5.4 Cross section measurements on water

420 In the water target events, the background from interaction with scintillators has to be
 421 subtracted by using the measurement of the hydrocarbon target.

Table 1: Expected number of the neutrino-candidate events in two WAGASCI modules after the event selections with 1×10^{21} POT in neutrino-mode.

Cut	CC	NC	Scinti Bkg.	Total
Reconstructed	45233	1749.27	9396.46	56378.8
FV	37876.8	1471.02	7869.57	47217.4
Pene. iron	28160.7	593.267	5750.79	34504.7
Stop/Penetrate MRDs	21195.4	534.914	4346.06	26076.4
after all cuts	81.3 %	2.1 %	16.7 %	100 %

Table 2: Expected number of the antineutrino-candidate events in two WAGASCI modules after the event selections with 1×10^{21} POT in antineutrino-mode.

Cut	CC	NC	Scinti Bkg.	Wrong sign bkg	Total
Reconstructed	16249.1	268.082	4468.83	5826.95	26813.0
FV	13644.7	223.211	3746.85	4866.36	22481.0
Pene. iron	10430.8	76.9422	2881.81	3901.35	17290.9
Stop/Penetrate MRDs	8328.73	71.2382	2240.59	2802.98	13443.5
after all cuts	62.0 %	0.5 %	16.7 %	20.9 %	100 %

422 **5.4.1 Charged current cross section measurement**

423 **6 Standalone WAGASCI-module performances**

424 In the previous sections, the WAGASCI detector was studied using the Muon Range Detectors. In this section, the standalone abilities of WAGASCI module are presented. Using
 425 the WAGASCI configuration presented in Section 5, we have evaluated that only 7% of
 426 the muons will be stopped in one of the WAGASCI modules. THowever, this proportion
 427 increases to 53% for pions and 73% for protons produced by neutrino interactions at 1.5°
 428 off-axis. Figure 28 shows the momentum distribution of these daughter particles as well as
 429 for the sub-sample stopped in one of the WAGASCI modules. Therefore, the study of the
 430 standalone abilities of the WAGASCI module in this section are dominantly motivated by:
 431

- 432 • the accurate measurement of the neutrino interaction final states. Though most of the
 433 muons will be reconstructed and identified in the MRDs, the hadronic particles will
 434 predominantly stops in one WAGASCI module. One has therefore to rely exclusively
 435 on the WAGASCI module information alone to reconstruct, identify and measure the
 436 momentum of pions or protons.
- 437 • the coverage of the MRDs is not 4π . Using the WAGASCI module information can

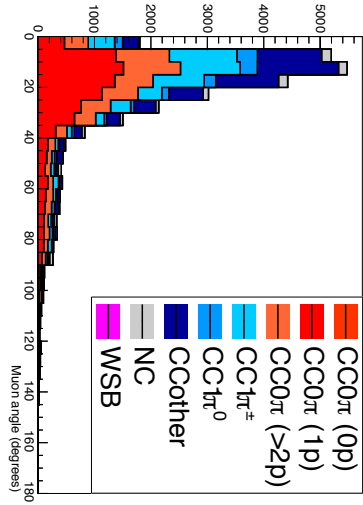


Figure 24: The reconstructed angles of the longest tracks in the selected events in the neutrino-mode.

438 therefore help to constraint the particles that exits the WAGASCI module but do
 439 not geometrically enters any MRD.

- 440 • the particle identification of low momenta $p_\mu < 300$ MeV/c that will leave only
 441 few hits in the MRD. Using the WAGASCI module information will clearly enhance
 442 the particle identification.

443 This study is based on an original study done for the ND280 upgrade target, with some
 444 modifications. Though the cell size is similar to the WAGASCI configuration presented
 445 in Section 5, the external dimensions are different ($186.4 \times 60 \times 130$ cm 3). Whenever the
 446 results are presented with this external size and this parameter is likely to impact the
 447 result, it will be mentioned.

448 Note that in this section, a simplified reconstruction algorithm presented in Section 6.1 is
 449 used. The fiducial volume is chosen accordingly as the inner cube of the module which
 450 surfaces are distant of $4 \times$ scintillator space = 10 cm from the module external surfaces.
 451 The neutrino interactions are simulated using NEUT v5.3.2. The NEUT input neutrino
 452 flux is estimated using JnuBeam v13a and assuming the detector to be located at 1.5°
 453 off-axis, as in Section 5. Note that the event reconstruction efficiency as a function of true
 454 neutrino energy might be changed at 1.5° , due for example to different Q^2 distributions. For
 455 this reason, one has to note that the reconstruction results might slightly be changed from
 456 2.5° and 1.5° . To avoid a similar change on the particle-only reconstruction efficiencies,

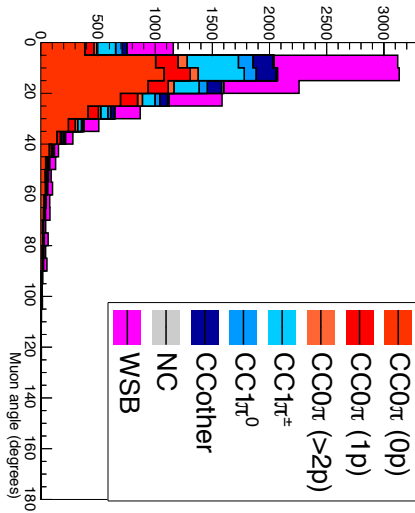


Figure 25: The reconstructed angles of the longest tracks in the selected events in the antineutrino-mode.

they will be presented as a function of variables that completely characterize the particle kinematic state, *i.e.* its momentum and angle. Figure 29 shows the vertices distributions of the daughter particles of neutrinos interacting one standard WAGASCI water-module. In this section, we will show the detector reconstruction and particle identification in this phase space, both for leptonic and hadronic particles. We will finally show an empty WAGASCI module can highly enhance the ability to constrain the neutrino interaction final state which is critical to reduce the corresponding uncertainties.

6.1 Reconstruction algorithm

6.1.1 Description

For this section, an ideal “simulated” reconstruction is developed. A particle is reconstructed if:

1. The particle is charged.
2. Lets at least one hit (energy deposit > 2.5 photo-electron) in a scintillator.
3. The particle enters one TPC and let one hit in the tracker.
Or

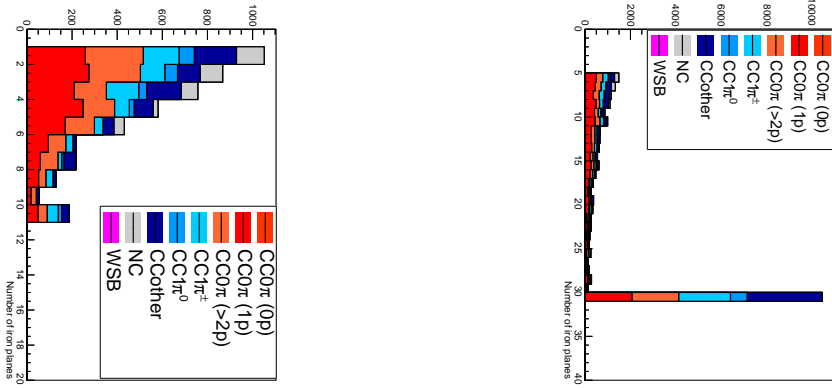


Figure 26: Iron plane numbers in Side-MRD (left) and Baby-MIND (right) corresponding to the end points of the longest tracks in the selected events in the neutrino-mode.

473

474

- The particle should be long enough to be reconstructed by the detector in at least 2 out of 3 views (XZ, YZ, XY). The length criterion requires the particle to let at least 4 hits in the detector. In the “less favourable case” of pure longitudinal or transverse going tracks, it represents a the track length of $L_{track} \geq 4 \times$ scintillator space = 10.0 cm.
- In the views where particles pass the length criterion, the particle shall not be superimposed with longer tracks in at least two views. The superposition criterion is estimated with the distance inter-tracks (DIT) which corresponds to the orthogonal distance between two tracks at the ending point of the shortest one (see Figure 30). For a track 1, the superposition criterion is tested with every longer tracks that starts at the same vertex. Let \vec{p}_1 the vector of track 1, and p_1^a its projections in the XZ, YZ and XY planes respectively for $i=1,2,3$. Note that these are projections in a 2D planes and not on a direction vector. In this case, the relative angle between the track 1 and a longer track 2 (of vector \vec{p}_2) in a view a is given by:

$$\cos \theta = \frac{\vec{p}_1^a \cdot \vec{p}_2^a}{\|\vec{p}_1^a\| \|\vec{p}_2^a\|} \quad (1)$$

489

and the distance inter track is given by:

$$DIT = \|\vec{p}_1^a\| \sin \theta \quad (2)$$

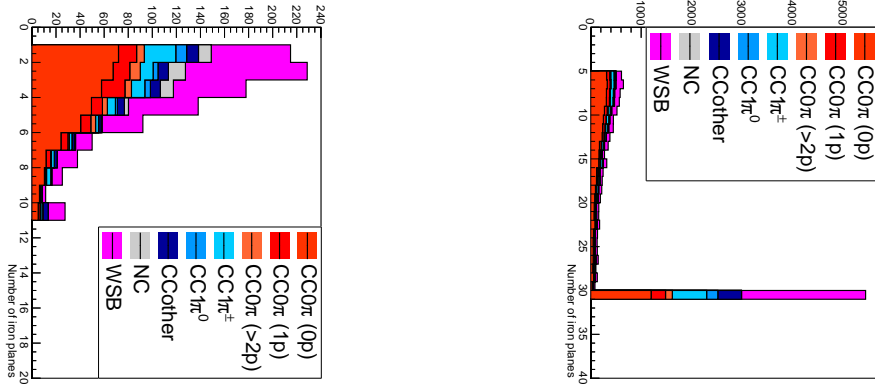


Figure 27: Iron plane numbers in Side-MRD (left) and Baby-MIND (right) corresponding to the end points of the longest tracks in the selected events in the antineutrino-mode.

490 The DIT should be higher than $4 \times$ scintillator width for the track 1 to be not
 491 superimposed with the track 2 in the view a, which also corresponds to 10.0 cm
 492 in the nominal configuration.

493 **6.1.2 Performances**

494 The particle-only reconstruction efficiencies and the reconstruction threshold in momenta
 495 are shown in Table 3. This threshold is defined as the maximal momentum for which the
 496 reconstruction efficiency is smaller than 30%. The thresholds in muon and pion momenta
 497 are 150 MeV/c. Most of the muons are above this threshold (see Figure 29) which leads
 498 to a 79% reconstruction efficiency.

	μ	π	p
Reconstruction Efficiency Momentum threshold	79% 150 MeV/c	52% 150 MeV/c	26% 550 MeV/c

Table 3: Reconstruction efficiency and momentum threshold for muons, pions and protons. The threshold is defined as the maximal momentum for which particles have a reconstruction efficiency smaller than 30%.

499 The lower pion and proton efficiencies (respectively 52% and 26%) are due to lower
 500 efficiencies for similar momenta than muons, coming from strong interactions as shown
 501 on Figures 31. Efficiencies of each particle type tend to decrease in the backward region

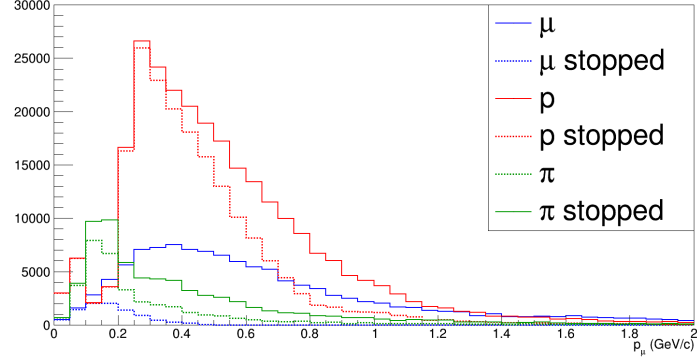


Figure 28: Momentum distribution of true particles in WAGASCI (plain) and corresponding distributions only for particles stopping into the WAGASCI module (dashed).

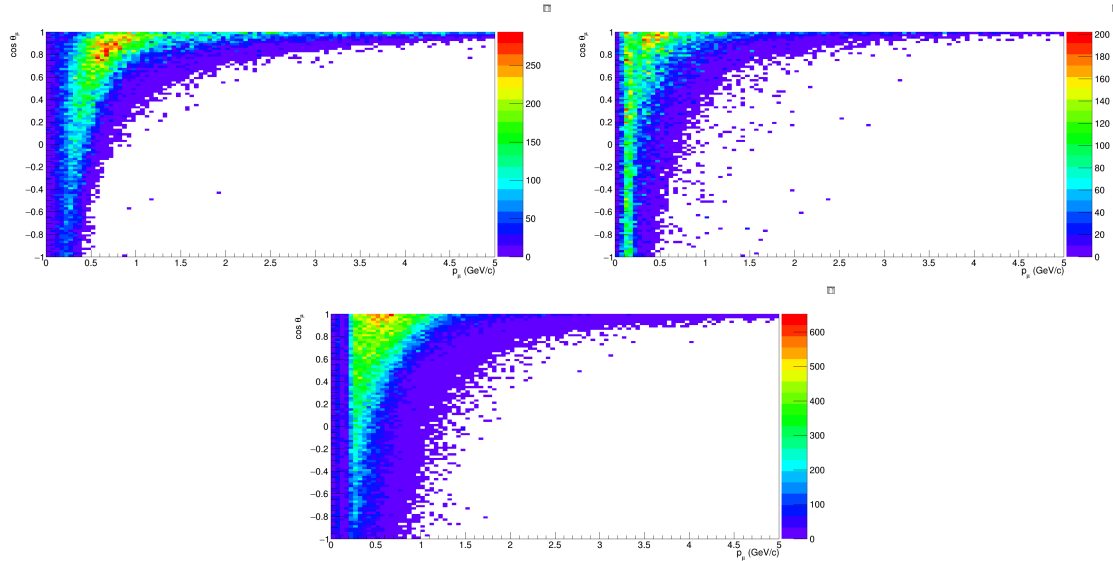


Figure 29: True number of muons (left), charged pions (right) and protons (bottom) in the two WAGASCI water-module as a function of the particles momenta and angles at 1.5° .

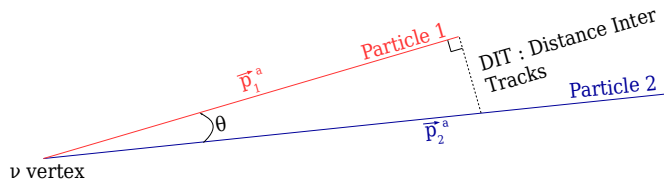


Figure 30: Definition of the distance inter tracks.

due to particle lower momenta. However, for a fixed momentum value, the reconstruction efficiency is almost uniform which confirms the ability of the WAGASCI detector to reconstruct high angle tracks.

The reconstruction is thereafter tested on neutrino events. Table 4 summarizes the number of reconstructed events and efficiencies for each interaction type. As expected from the high muon reconstruction efficiency, the charged current interactions have reconstruction efficiencies $\geq 85\%$.

	CC0π	CC1π	CCOthers	NC	All
Reconstruction efficiency	85%	87%	91%	22%	68%

Table 4: Number of true interactions reconstructed. The purity and reconstruction efficiency of each true interaction is also shown.

The reconstruction efficiencies as a function of the neutrino energy and muon kinematics are respectively shown on Figure 32 and 33.

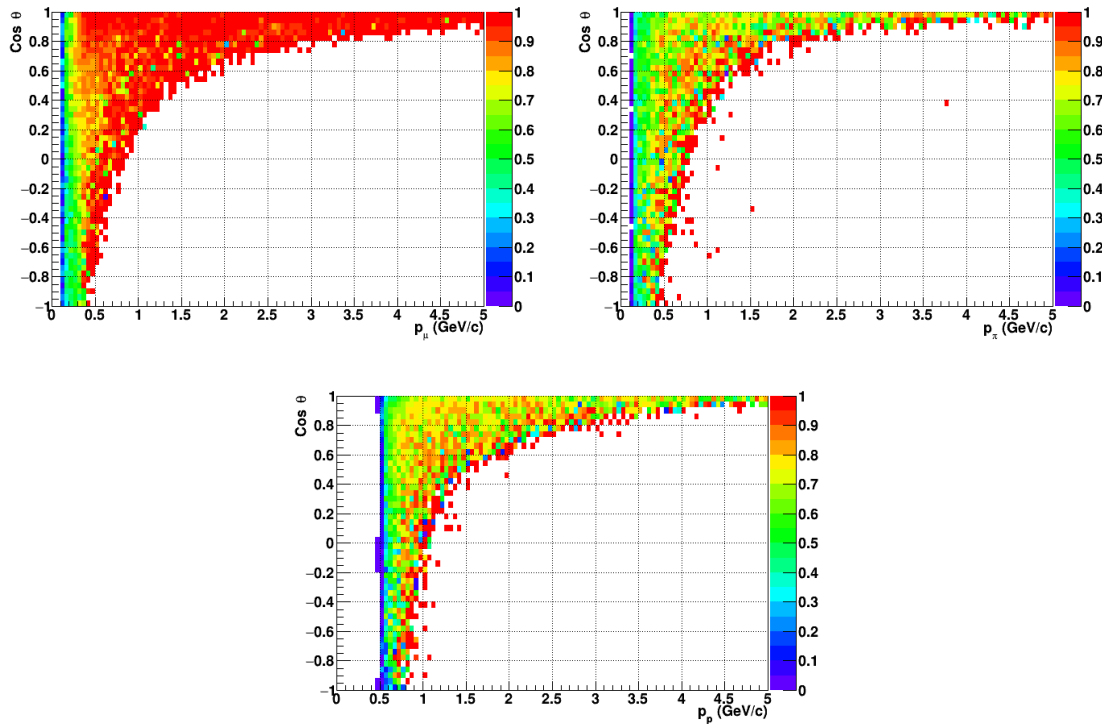


Figure 31: Reconstruction efficiency of muons (left), charged pions (right) and protons (bottom) in the WAGASCI water-module as a function of the particles momenta and angles.

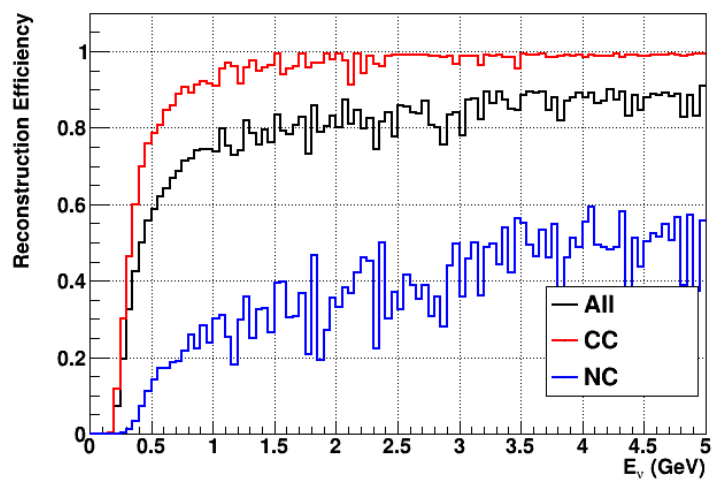


Figure 32: Reconstruction efficiency of all neutrino (black), CC (red) and NC (blue) interactions in the WAGASCI water-module as a function of the neutrino energy.

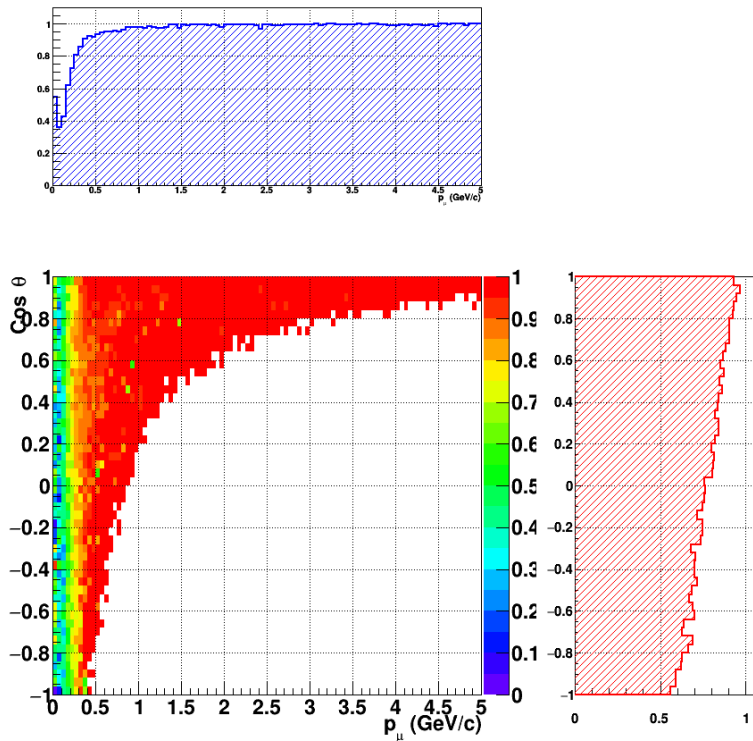


Figure 33: Reconstruction efficiency of CC interactions in the WAGASCI water-module as a function of the muon kinematic variables (momentum and angle).

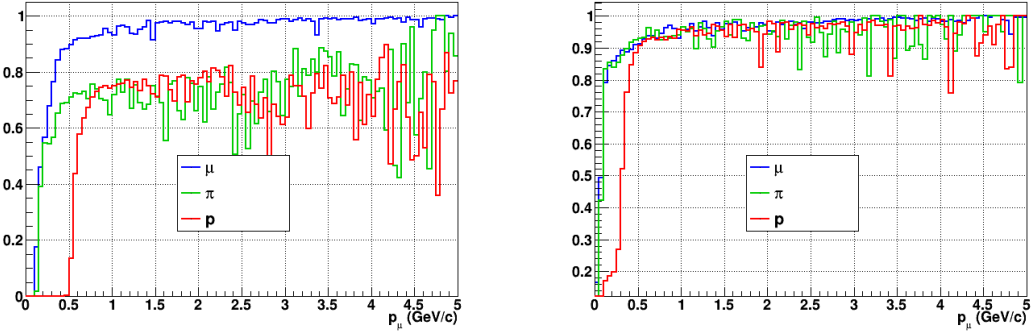


Figure 34: Reconstruction efficiency for muons, pions and protons in the water-in (left) and water-out (right) modules.

511 Note that a Particle Identification Algorithm has been also developed. It is based on
 512 the charge deposition of the particles in the scintillator, of the detection of a decay-electron.
 513 However, this information highly depends on the number of scintillator hit by a particle,
 514 which creates an important difference between a real WAGASCI module and the one used
 515 for the ND280-upgrade simulation. For this reason, the corresponding results will not be
 516 detailed here, but can be found in [?].

517 6.2 Background subtraction: the water-out module

518 In the nominal configuration, 20% of the neutrino interactions occurs on scintillators
 519 (C_8H_8). This background should be removed in order to measure the neutrino interac-
 520 tion on the same target as Super-K, which suppress the differences in cross-section models.
 521 For this purpose, we propose to use a water-out module, where the water is replaced by
 522 air. The detector is therefore fully active and has a 3 mm spatial resolution (scintillator
 523 thickness) which create an ideal detector to reconstruct and identify hadrons, and study
 524 np-nh interactions. The counter-part is the difference in particle energy deposition between
 525 the water and this water-out module that will need to be corrected for. In this section,
 526 we present the capabilities of such a module, and the impact it can have on cross-section
 527 measurements for the neutrino community in general and T2K in particular.
 528 The same reconstruction and selection as the water-in module is applied. Figure 34 shows
 529 the comparison between the water-in and the water-out reconstruction efficiencies for muon,
 530 pions and protons. 90% of the muons and 87% of the pions are reconstructed, while 70%
 531 of the protons are even reconstructed. It allows to lower down the proton threshold to
 532 250 MeV/c (see Table 5).

533 As a consequence of tracking even low momenta particle, the reconstruction efficiency
 534 is uniform and almost maximal on the entire $\cos \theta_\mu$ phase space, as shown on Figure 35.

	μ	π	p
Reconstruction Efficiency Momentum threshold	90% 50 MeV/c	87% 50 MeV/c	70% 250 MeV/c

Table 5: Reconstruction efficiency, proportions of μ -like and non μ -like and momentum threshold for muons, pions and protons in the empty module. The threshold is defined as the maximal momentum for which particles have a reconstruction efficiency smaller than 20%.

535 Since the fiducial mass represents 0.25 tons, the total number of events is divided by a
 536 factor of 3 compared to the water-in module. The water-out module offers interesting
 537 possibilities to study np-nh interaction since 70% of the protons are reconstructed. In the
 538 future, a possible separation as a function of the number of proton track will be studied.
 539 Moreover, we are currently pursuing the use of single and double transverse variables (cite
 540 Xianguo) to open new possibilities for separating np-nh from Final State Interactions, or
 541 for isolating the interactions on hydrogen from interactions on carbon in this module.

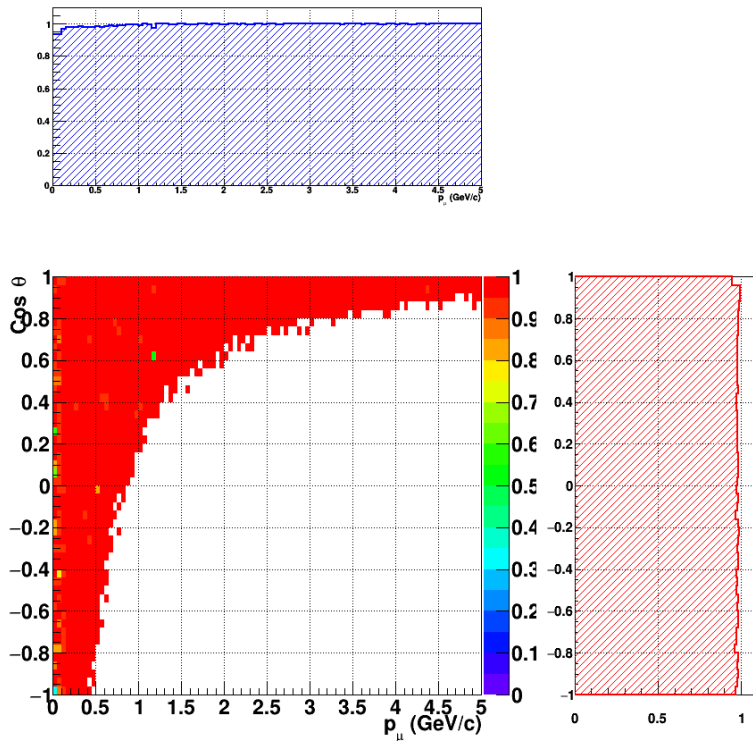


Figure 35: Reconstruction efficiency of CC interactions in the WAGASCI empty module as a function of the muon kinematic variables (momentum and angle).

542 **7 Schedule**

543 We would like to start a physics data taking from T2K beam time after the summer
544 shutdown in 2018. By then, commissioning and tests of the detectors will be completed
545 in J-PARC T59. The experiment can run parasitically with T2K, therefore we request no
546 dedicated beam time nor beam condition as discussed in the following section.

547 Once the approved POT is accumulated, the WAGASCI modules will be removed
548 from the experimental site, but we would like to keep the Baby-MIND and the Side-MRD
549 modules on the B2 floor of the NM pit as common platforms of future neutrino experiments
550 using the T2K neutrino beam.

551 **8 Requests**

552 **8.1 Neutrino beam**

553 The experiment can run parasitically with T2K, therefore we request no dedicated beam
554 time nor beam condition. As data taking periods, we request the ‘nominal’ T2K one-year
555 operation both for the neutrino beam and the antineutrino beam. The T2K has been
556 requesting 0.9×10^{21} POT/year and actually accumulating about 0.7×10^{21} POT/year in
557 recent years. For each year, starting from the Autumn, T2K is running predominantly in
558 the neutrino mode or in the antineutrino mode. Our request is to have one-year neutrino-
559 mode data and another one-year antineutrino mode data assuming that the POT for the
560 fast extraction in each year is more than 0.5×10^{21} POT.

561 **8.2 Equipment request including power line**

562 We request the followings in terms of equipment on the B2 floor:

- 563 • Site for the WAGASCI modules, Side-MRD modules and BabyMIND and their elec-
564 tronics system on the B2 floor of the near detector hall (Fig. 2).
- 565 • Anchor points (holes) on the B2 floor to secure the WAGASCI modules, Side-MRD
566 module and Baby-MIND (Fig. ??)
- 567 • Power line for the magnets in Baby-MIND: 400 V tri-phase 48-to-62 Hz, capable of
568 delivering 12 kW.
- 569 • Electricity for electronics and water circulation system, 3 kW, standard Japanese
570 electrical sockets.
- 571 1. Online PCs: 2.1 kW
- 572 2. Electronics: 0.7 kW
- 573 3. Water sensors: ?

- 574 • Air conditioner for cooling heat generation at Baby-MIND magnets, online PCs and
575 electronics
- 576 • Beam timing signal and spill information
- 577 • Network connection

578 **8.2.1 Baby MIND Equipment request including power line**

579 We request the following in terms of equipment on the B2 floor:

- 580 • Site for the Baby MIND detector and its electronics systems on the B2 floor of the
581 near detector hall.
- 582 • Anchor points (holes) on the B2 floor to secure the 9 support frames, of order 4 holes
583 per frame, detailed floor plans to be communicated in a separate document.
- 584 • Power line for the magnet: 400 V tri-phase 48-to-62 Hz, capable of delivering 12
585 kW. We have a wish for the magnet power line to be installed and available to us by
586 beginning of March 2018.
- 587 • Electricity for electronics, 1 kW, standard Japanese electrical sockets.
- 588 • Beam timing signal and spill information
- 589 • Network connection

590 The infrastructure for much of the above exists already, and will be shared in part with
591 the WAGASCI experiment. Exceptions are the power line for the magnet and holes in the
592 B2 floor to anchor the detector support structures.

593 **9 Conclusion**

594 **References**

- 595 [1] K. Abe et al. Measurement of the muon neutrino inclusive charged-current cross sec-
596 tion in the energy range of 13 GeV with the T2K INGRID detector. *Phys. Rev.*,
597 D93(7):072002, 2016.
- 598 [2] M. Antonova et al. Baby MIND Experiment Construction Status. In *Prospects in*
599 *Neutrino Physics (NuPhys2016) London, London, United Kingdom, December 12-14,*
600 2016, 2017.

- 601 [3] J. Fleury, S. Callier, C. de La Taille, N. Seguin, D. Thienpont, F. Dulucq, S. Ahmad,
602 and G. Martin. Petiroc and Citiroc: front-end ASICs for SiPM read-out and ToF
603 applications. *JINST*, 9:C01049, 2014.
- 604 [4] Yu. G. Kudenko, L. S. Littenberg, V. A. Mayatsky, O. V. Mineev, and N. V. Ershov.
605 Extruded plastic counters with WLS fiber readout. *Nucl. Instrum. Meth.*, A469:340–
606 346, 2001.
- 607 [5] O. Mineev, Yu. Kudenko, Yu. Musienko, I. Polyansky, and N. Yershov. Scintillator
608 detectors with long WLS fibers and multi-pixel photodiodes. *JINST*, 6:P12004, 2011.
- 609 [6] Etam Noah et al. Readout scheme for the Baby-MIND detector. *PoS*, Photo-
610 toDet2015:031, 2016.